Journal of Solid Mechanics Vol. 14, No. 3 (2022) pp. 377-397
DOI: 10.22034/jsm.2021.1929984.1696

Research Paper

Investigating Stress Intensity Factor and Fatigue Life Using Extended Isogeometric Analysis Based on Bézier Extraction of NURBS

M.M. Shoheib [1], Sh. Shahrooi [1,*], M. Shishehsaz [2], M. Hamzehei [1]

[1] *Department of Mechanical Engineering, Ahvaz Branch, Islamic Azad University, Ahvaz, Iran*
[2] *Department of Mechanical Engineering, Faculty of Engineering, Shahid Chamran University of Ahvaz, Ahvaz, Iran*

Received 8 June 2022; accepted 10 August 2022

ABSTRACT

In this paper, the extended isogeometric analysis based on Bézier extraction of NURBS is applied for Investigating stress intensity factor and fatigue life in the two-dimensional crack problems with thermal and mechanical cyclic loading. By transforming NURBS function to linear combination of Bernstein functions defined over C^0-continuous Bézier elements, the extended isogeometric analysis can be implemented in the extended finite element method framework. Grid points around the crack line and crack tip are identified by the level set representation. Then, discontinuous enrichment functions are added to the isogeometric analysis approximation. Thus, this method does not require remeshing. The interaction integral method and Paris law has been used to extract stress intensity factor and evaluate fatigue life, respectively. Numerical examples are examined to validate the efficiency of the proposed method. The effect of adaptive refinement strategies on computational cost and convergence is studied. Numerical examples showed that the presented method produces highly accurate results, yet it is beneficial to implement.

Keywords : XIGA analysis; Bézier extraction operator; Cyclic load; Stress intensity factor; Fatigue life.

1 INTRODUCTION

CRACK propagation analysis by numerical modeling has been a challenge for researchers during the past and recent years. More numerical methods were based on a discrete crack analysis that used remeshing approach due to boundary requirements in the new generated elements introduced by the crack increments. Many different approaches have been presented to overcome the difficulties of crack geometric topological changes and remeshing during crack propagation, such as combinative methods for crack modeling and analyzing [1,2], extended finite element method [3,5] and meshfree methods [6-8]. These methods were developed to reduce the computational cost

*Corresponding author.
E-mail address: shahramshahrooi@iauahvaz.ac.ir (S. Shahrooi)

and remeshing steps and enable these methods to handle crack propagation and discontinuous problems. The isogeometric analysis uses a geometric basis function, as used in computer-aided design, within the modeling and analysis process. The fundamental basis function in CAD is B-spline or NURBS. The advantage of isogeometric analysis method is to use the same basis function for modeling and analysis. The IGA method allows us to create the exact geometry by few elements and solution results with higher accuracy [9]. Bhardwaj *et al*. [10,11] used the XIGA to evaluate fracture behavior of cracked plates under static loading for different boundary conditions. Tran *et al*. [12] employed the IGA for the buckling, static and dynamic response of plates. Huang *et al*. [13] performed Analytical characterizations of crack tip stress field and crack tip plastic zone for central cracked unstiffened and stiffened plates. Gadallah *et al*. [14] presented a new method to compute the mixed-mode SIFs for a through-thickness crack in a welded medium with a residual stress field. Yuan *et al*. [15] studied Mode I stress intensity factor for cracked special-shaped shells under bending load. However, the isogeometric analysis method has been investigated richly by many researchers. There still exists an incompatibility between the volumetric representation of geometries and the boundary representation of the CAD models. To overcome this difficulty, Bézier extraction operator approach can be used with the isogeometric analysis. In general, NURBS basis functions span over the entire domain of geometries (models) and do not possess a local domain (element) as Lagrange shape functions. The global structure requires complex implementation within the traditional IGA context. Computation of stiffness matrix formulation needs to be further transformed into the parent element while the basis functions are defined in the parametric space. By choosing Bernstein functions as the basis functions in Bézier extraction, the isogeometric analysis will be performed similarly to what was done in traditional finite element. The Bernstein functions have the C^0-continuity similar to Lagrange shape functions. The Bézier extraction operator allows the incorporation of non-uniform rational B-spline based isogeometric analysis into the traditional finite element method framework. Cimrman et al. [16] performed a convergence study of IGA based on Bézier extraction in electronic structure. They explained a new method for non-periodic electronic structures based on the density functional theory, environment reflecting pseudo potentials and the IGA using Bézier extraction, ensuring continuity for all quantities up to the second derivative. Lieu B. Nguyen et al. [17] employed isogeometric Bézier with a C^0-type shear deformation theory for structural vibration analysis of functionally graded piezoelectric porous plates. They have shown that the results of this method match very well with the similar numerical studies or other solutions. Kumar *et al*. [18] studied stress intensity factor on crack tip plastic zones by the XIGA. This study shows the effect of holes on the extent of crack. Shuohui *et al*. [19] developed a novel method for simulating static and dynamic crack problems in 2D elastic solids through a XIGA. Their method provides several advantages in fracture modeling and analysis.

In this study, the XIGA approach based on Bézier extraction is used to analyze the crack propagation in a plate with thermal and mechanical cyclic loading, for the purpose of SIFs extraction, determination of fatigue life and the adaptive refinement strategies. For this purpose, the concepts of enrichment were used to enrich the IGA control points with Heaviside and crack tip enrichment functions. Finally, several numerical examples considering the geometry, boundary and loading conditions are introduced, results on which are compared with other approaches. In Section 2 of this paper, the framework of IGA is discussed. The B-spline and NURBS basis functions, Bézier extraction of NURBS and the extended isogeometric analysis that govern a crack problem in a linear elastic fracture mechanic are also introduced. Section 3 presents the interaction integral method for computation of stress intensity factor. The crack growth and fatigue life- related work are detailed in Section 4. Fundamental equations of thermo-elastic problems are given in Section 5. Section 6 describes the various numerical examples for evaluating the stress intensity factor and the fatigue life of a cracked plate to verify the accuracy of the method.

2 ISOGEOMETRIC ANALYSIS METHOD

2.1 B-spline and NURBS basis functions

The B-spline basis functions are fundamental concepts of establishing IGA, which could be expressed by a set of knot values called knot vector, $\Xi = \{\xi_1, \xi_2, ..., \xi_{n+p+1}\}$ ($\xi_i \in R$), where n is the number of basis functions and p is the polynomial order. The B-spline basis functions are defined by the following recursive forms [11].

$$N_{i,0} = \begin{cases} 1 & \xi_i \le \xi \le \xi_{i+1} \\ 0 & otherwise \end{cases} \quad \text{for } p = 0 \tag{1}$$

$$N_{i,p}(\xi)=\frac{\xi-\xi_i}{\xi_{i+p-1}-\xi_i}N_{i,p-1}(\xi)+\frac{\xi_{i+p}-\xi}{\xi_{i+p}-\xi_{i+1}}N_{i+1,p-1}(\xi) \quad \text{for} \quad p>0 \tag{2}$$

NURBS basis function is for exactly present the conical sections such as circle and ellipse that defined as:

$$R_{i,p}(\xi)=\frac{w_i N_{i,p}(\xi)}{W(\xi)}=\frac{N_{i,p}(\xi)w_i}{\sum_{i=0}^{n}N_{i,p}(\xi)w_i} \tag{3}$$

Also the two dimensional NURBS are defined as:

$$R(\xi,\eta)=\frac{N_{i,p}(\xi)M_{j,q}(\eta)w_{i,j}}{\sum_{i=0}^{n}\sum_{j=0}^{m}N_{i,p}(\xi)M_{j,q}(\eta)w_{i,j}} \tag{4}$$

2.2 Bézier extraction of NURBS

In this section, the method of constructing the NURBS function using Bézier elements and the Bézier extraction operator is presented. The Bézier element spans traditionally [0,1] (in each direction) and is created by a knot vector without the internal knot. The knot vector contains (p+1) zeros and ones, where p is the polynomial order. The basis functions created by this kind of knot vector are named the Bernstein functions and have many similarities to the Lagrange basis functions that used in finite element method. Besides, the Bernstein functions can be defined over the interval [−1,1] such that the Bézier element spans the same interval as the quadrilateral elements in FEM. Since the knot values are restricted to −1 and 1 and each one of them is repeated (p+1) times, then the Bernstein functions defined as [20]:

$$B_{i,p}(\xi)=\frac{1}{2}(1-\xi)B_{i,p-1}(\xi)+\frac{1}{2}(1+\xi)B_{i-1,p-1}(\xi) \tag{5}$$

where,

$$B_{1,0}(\xi)=1\ ,\ B_{i,p}(\xi)=0 \quad if \quad i\langle 1 \quad , \quad i\rangle p+1 \tag{6}$$

These Bernstein functions, similar to the B-splines and NURBS functions, constitute the partition of unity and are nonnegative over the entire domain. In addition, The Bernstein functions identical to the Lagrange functions are symmetric and interpolator at the endpoints of the domain. The Bézier curve evaluated by a linear combination of Bernstein functions and control point coordinates set as:

$$C(\xi)=\sum_{i=0}^{p}B_i^p(\xi)P_i=P^T B(\xi) \tag{7}$$

Bézier extraction operator maps the linear combinations of Bernstein functions into NURBS basis functions. Using this transformation, it is possible to use piecewise C^0 Bézier elements as the FEM in isogeometric analysis. To decompose a set of NURBS basis functions to its Bézier elements, called Bézier decomposition, all internal knots of the knot vector are repeated until they have a multiplicity equal to p (polynomial order). In fact, the interior knots should have a multiplicity of (p+1) to create correctly separated Bézier elements. The multiplicity of p is enough to present the Bernstein functions, which in this study are also referred to as Bézier basis functions. The curves and surface created by the NURBS basis functions and as well as the Bézier basis functions are entirely similar but the number of control points increases similar to the number of basis functions while their location are changed.

Considering that the Bézier decomposition is a knot insertion operation, the Bézier extraction operator is based on the equations of new control points created by the original control points when a knot is inserted. Assuming $\xi \in$

$[\xi_k, \xi_{k+1}]$ & $(k > p)$ is a new knot inserted into the existing knot vector $\Xi = \{\xi_1, \xi_2, \ldots, \xi_{n+p+1}\}$, then, the new set of control points are created as [16]:

$$\bar{P}_i = \begin{cases} P_1 & i = 1 \\ \alpha_i P_i + (1-\alpha_i) P_{i-1} & 1 < i < m \ , \ m = n+1 \\ P_n & i = m \end{cases} \tag{8}$$

$$\alpha_i = \begin{cases} 1 & i \le K - P \\ \dfrac{\bar{\xi} - \xi_k}{\xi_{i+p} - \xi_i} & K - P + 1 \le i \le K \\ 0 & i \ge K + 1 \end{cases} \tag{9}$$

where P_i and $\bar{P}_i$ are the existing and new control points, respectively.

According to the operation of knots insertion, given a new set of knots $\{\xi_1, \xi_2, \ldots, \xi_m\}$, the Bézier extraction operator C_j (j =1,2,...,m) can be determined in a matrix form as:

$$\boldsymbol{C}_j = \begin{bmatrix} \alpha_1 & 1-\alpha_2 & 0 & & 0 \\ 0 & \alpha_2 & 1-\alpha_3 & \cdots & 0 \\ 0 & 0 & \alpha_3 & & 0 \\ & \vdots & & \ddots & \vdots \\ 0 & 0 & 0 & \cdots & \alpha_{(n+j-1)}(1-\alpha_{(n+j)}) \end{bmatrix} \tag{10}$$

Consequently, Eq. (8) can be recast in a matrix form to present the sequence of control points created by the knot insertion operation.

$$\bar{\boldsymbol{P}}_{j+1} = \left(\boldsymbol{C}_j\right)^T \bar{\boldsymbol{P}}_j \quad \text{where} \quad \bar{P}_1 = P \tag{11}$$

The final control points $\bar{\boldsymbol{P}}_{m+1} = \boldsymbol{P}_b$ are explained as:

$$\boldsymbol{C}^T = (\boldsymbol{C}_m)^T (\boldsymbol{C}_{m-1})^T \ldots (\boldsymbol{C}_1)^T \tag{12}$$

Moreover, the relation between new Bézier control points and the original NURBS control points is defining as:

$$\bar{\boldsymbol{P}} = \boldsymbol{C}^T \boldsymbol{P} \tag{13}$$

Considering the knot insertion causes no change in parametric or geometric nature of the curve, then, one can write,

$$C(\xi) = \left(\bar{P}\right)^T B(\xi) = (C^T P)^T B(\xi) = P^T C B(\xi) = P^T N(\xi) \tag{14}$$

Therefore, the relation between the B-spline basis functions and the Bernstein functions can be expressed as:

$$\boldsymbol{N}(\xi) = \boldsymbol{C}\,\boldsymbol{B}(\xi) \tag{15}$$

In above equation, $\boldsymbol{C}$ is called the Bézier extraction operator. In Bézier extraction, the NURBS basis functions are expressed with Bernstein functions. The only input required to calculate $\boldsymbol{C}$ is the knot vector. Therefore, the

Bézier extraction operator is independent from control points as well as the basis functions. This means that the Bézier extraction operator is the same for B-splines and NURBS.

To define the bivariate Bézier extraction operators suppose that $\mathbf{C}_{\xi}^{\mathrm{i}}$ and $\mathbf{C}_{\eta}^{i}$ are the *ith*, *jth*, univariate Bézier extraction operators in the ξ and η directions. Then the bivariate extraction operator is defined as:

$$\mathbf{C}_{\mathrm{A}}^{\mathrm{e}} = \mathbf{C}_{\xi}^{\mathrm{i}} \otimes \mathbf{C}_{\eta}^{\mathrm{i}} \tag{16}$$

where $\otimes$ is defined for the two matrices **A** and **B**, which may have different dimensions as:

$$\mathbf{A} \otimes \mathbf{B} = \begin{bmatrix} \mathrm{A}_{11}\mathrm{B} & \mathrm{A}_{12}\mathrm{B} & \cdots \\ \mathrm{A}_{21}\mathrm{B} & \mathrm{A}_{22}\mathrm{B} & \cdots \\ \vdots & \vdots & \ddots \end{bmatrix} \tag{17}$$

To obtain the NURBS basis functions, the weighting function is written as:

$$\mathbf{W}(\xi) = \sum_{i=1}^{n} N_{i,p}(\xi)\mathcal{W}_i = \boldsymbol{w}^T \boldsymbol{N}(\xi) = \boldsymbol{w}^T \mathbf{C}\mathbf{B}(\xi) = \left(\boldsymbol{C}^T \boldsymbol{w}\right)^T \boldsymbol{B}(\xi) = \left(w_b\right)^T B(\xi) = W_b(\xi) \tag{18}$$

In Eq. (18), $\boldsymbol{w}_b = \boldsymbol{C}^T\boldsymbol{w}$ are the weights of the Bézier basis functions, given as a vector. Substituting Eq. (15) into Eq. (4), the NURBS basis functions using the Bernstein functions and the Bézier extraction operator defined as:

$$\boldsymbol{R}(\xi) = \frac{1}{\boldsymbol{W}_b(\xi)} \boldsymbol{W}\boldsymbol{C}\boldsymbol{B}(\xi) \tag{19}$$

where $\boldsymbol{W}$ is the NURBS weights. Since with the knot insertion, the Bézier decomposition of control points is performed directly to the NURBS curve. The relation between Bézier and NURBS control points is:

$$\mathbf{P}^{\mathrm{b}} = \left(\mathbf{W}_{\mathrm{b}}\right)^{-1} \mathbf{C}^{\mathrm{T}}\mathbf{W}\mathbf{P} \tag{20}$$

where, $\boldsymbol{W}_b$ is the Bézier weights and w_b is given in terms of as a diagonal matrix. By Multiplying Eq. (20) by $\boldsymbol{W}_b$

$$\mathbf{W}_{\mathrm{b}}\mathbf{P}^{\mathrm{b}} = \mathbf{C}^{\mathrm{T}}\mathbf{W}\mathbf{P} \tag{21}$$

Combining Eqs. (19) and (21), the NURBS curve in terms of C^0 Bézier elements is recast in Eq. (22). Similarly, the NURBS surface in terms of C^0 Bézier elements is expressed in Eq. (23).

$$C(\xi) = P^T R(\xi) = \frac{1}{\mathrm{W}_{\mathrm{b}}(\xi)} P^T W C B(\xi) = \frac{1}{\mathrm{W}_{\mathrm{b}}(\xi)} \left(\mathrm{W}_{\mathrm{b}} P^b\right)^T B(\xi) \tag{22}$$

$$S(\xi,\eta) = \frac{1}{\mathrm{W}_{\mathrm{b}}(\xi,\eta)} \left(W_b P^b\right) B(\xi,\eta) \tag{23}$$

2.3 Extended isogeometric analysis

2.3.1 Level set representation

In the level set technique, a crack is defined by two orthogonal level set fields [21]. One of these fileds define the crack line $\{x: \varphi(x) = 0$ and $\psi(x) \leq 0\}$, and the other one is used to define the crack tip $\{x: \varphi(x) = 0$ and $\psi(x) = 0\}$. This implicit definition of the crack line and the crack tip by the level set can be illustrated in Fig. 1.

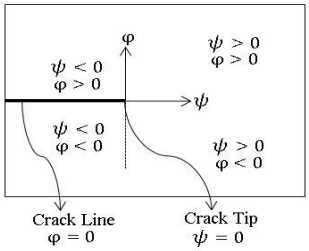

Fig.1
Crack line function φ and crack tip function ψ.

Quantity of the two level set functions are generated on control points around the crack line and crack tip, and used to obtain geometric information of the crack location and provides a local coordinate system that used to generate the enrichment functions used in the XIGA approach. This is accomplished as well by requiring that φ always represents the signed distance to the extended crack line, while ψ gives the signed distance to the line that intersects the crack line at the crack tip while being orthogonal to the crack line as well. To initialize the values of φ and ψ, we start by initializing φ on the control points of the elements that are cut by the extended initial crack line (Fig. 2).

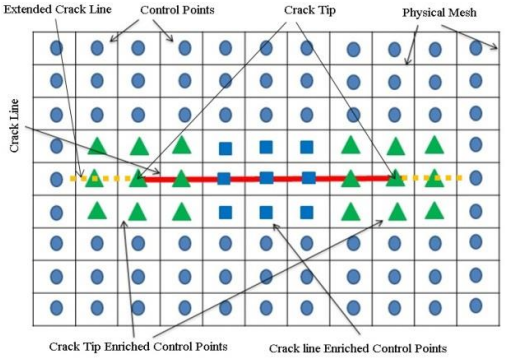

Fig.2
Illustration of points around the crack line.

For a given grid point, P, the value of φ is the minimum distance between P and the crack line. Assuming (x_0,y_0) and (x_1,y_1) represent the coordinates of the starting point and end point of a crack, and $P=(x,y)$ is the point on a special element where the minimum distance is obtained, and n is the unit normal to the element containing the point P, φ is initialized as,

$$\varphi=(x-y).n=\frac{(y_0-y_1)x+(x_1-x_0)y+(x_0y_1-x_1y_0)}{\sqrt{(x_1-x_0)^2+(y_1-y_0)^2}} \tag{24}$$

where φ is computed for each grid point to recognize the element cut by crack line. This extends φ, as the signed distance function, radially outward from the crack line. The crack tip function, ψ, determined as,

$$\psi=\left([xy]-[x_1y_1]\right).\left(\frac{(x_1-x_0)\vec{i}+(y_1-y_0)\vec{j}}{\left|(x_1-x_0)\vec{i}+(y_1-y_0)\vec{j}\right|}\right) \tag{25}$$

Similarly, the value of the level set function ψ is the minimum distance between each grid point and the crack tip. ψ is computed for each grid point (control points) of the model to recognize the element around the crack tip. Note that the values of φ and ψ are set only within a specified bandwidth, β, from the crack line. Thus, these values are set only for the grid points P such that $\psi(y) \leq \beta$ and $\varphi(y) \leq \beta$. Updating the level set functions φ and ψ is to reconstruct the crack tip from the intersection of the two isosurfaces, $\{x:\varphi(y)=0\}\cap\{x:\psi(y)=0\}$. On the other hand, for the split knot span (element) $Max(\varphi)\times\mathrm{Min}(\varphi)<0 \; and \; Max(\psi)<0$ and for the crack tip knot span (element) $Max(\varphi)\times Min(\varphi)<0 \;\; and \;\; Max(\psi)\times Min(\psi)<0$.

2.3.2 XIGA approximations for cracks

In the extended isogeometric analysis, the displacement approximation is locally enriched to simulate discontinuities. For this purpose, few fictitious nodes and their degrees of freedom are added to the selected control points near the location of a crack. The basic concept of XIGA is the extent of approximation of the basis functions by special enrichment functions selected according to the behavior of the crack problem. To model the cracks in XIGA, the elements divided by the discontinuities are recognized as the enriched elements. Furthermore, in the XIGA, the crack is represented independent of the meshing process and hence, remeshing is not required for the analysis of crack propagation. The level set technique is used to identify the enriched and nonenriched elements as well as their control points. The elements intersected by the crack line are called split elements while the elements intersected by the crack tips are named tip elements. There is one to one communication between the control points and the basis functions. Hence, each basis function can be uniquely assigned to its control point. Moreover, each basis function has its supported domain (control points) and becomes zero outside this domain. These specifications are unified to detect the control points related to the split and tip elements. The number of control points related to a split element or tip element depends on the order of basis functions. However, the change in the basis functions order changes the number of control points. The typical XIGA discretization with the enriched control points is shown in Figs. 3(a), and Fig. 3(b) for basis functions of orders 1 and 3, respectively.

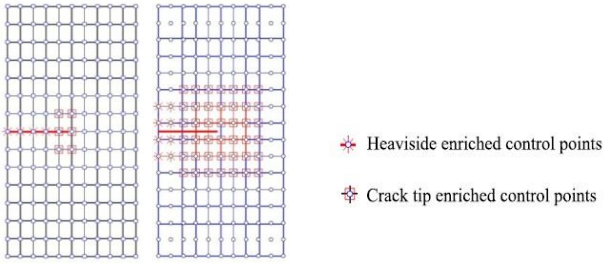

(a) (b)

Fig.3
Crack model with XIGA and enriched control points for (a) basis functions of order 1, and (b) basis functions of order 3.

The control points associated with the split elements and the tip elements are enriched with the Heaviside function and the crack tip enrichment functions, respectively. The XIGA approximations in the 2D continuum formulation for cracks are given as [22,23],

$$u^{\mathrm{h}}(\xi)=u^{IGA}(\xi)+u^{\mathrm{XIGA}}(\xi)=\sum_{\mathrm{i}=1}^{\mathrm{n}}\mathrm{R}_{\mathrm{i}}(\xi)\mathrm{u}_{\mathrm{i}}+u^{\mathrm{enrichment}} \tag{26}$$

The first term in Eq. (26) represents presents the standard isogeometric analysis approximation. Additionally, $R_i(\xi)$ is the basis functions and u_i are the standard degrees of freedom related to a special control point. Other terms in the displacement field are used to represent the discontinuous behavior by enrichment function. Eq. (26) can be expressed in terms of the Heaviside function and crack tip enrichment functions as:

$$u(\xi)=\sum_{i=1}^{n_{el}}\mathrm{R}_{\mathrm{i}}(\xi)\mathrm{u}_{\mathrm{i}}+\sum_{j=1}^{n_h}\mathrm{R}_{\mathrm{i}}(\xi)\left[H(\xi)-H(\xi_i)\right]a_j+\sum_{k=1}^{n_t}\mathrm{R}_{\mathrm{k}}(\xi)\left\{\sum_{\alpha=1}^{4}\left[\mathrm{Q}_{\alpha}(\xi)-\mathrm{Q}_{\alpha}(\xi_i)\right]b_k^{\alpha}\right\} \tag{27}$$

where (R_i) are the basis functions; $H(\xi)$s are the Heaviside functions and $Q_\alpha(\xi)$s are the asymptotic crack tip enrichment functions. Moreover, a_j and b_k^{α} are the additional degrees of freedom related to the modeling crack line and the crack tip, and n_h and n_t are the number of control points enriched with Heaviside and crack tip enrichment functions, respectively.

The Heaviside function $H(\xi)$ is equal to +1 or −1 depending on the location of the control point concerning the crack lines. For each individual control point in the particular element, the $H(\xi)$ is equal to +1 if the point lies above the crack line and -1 otherwise. The asymptotic crack tip enrichment functions are defined as:

$$\mathrm{Q}_{\alpha}(\xi)=\left\{\sqrt{r}\cos\frac{\theta}{2},\sqrt{r}\sin\frac{\theta}{2},\sqrt{r}\cos\frac{\theta}{2}\sin\theta,\sqrt{r}\sin\frac{\theta}{2}\sin\theta\right\} \tag{28}$$

where r and θ are the polar coordinates of a point concerned with the crack tip. Each split node is enriched by one function, $H(x)$. Each tip node is enriched by four functions, $Q_\alpha(\xi)$. Then, the total degrees of freedom is number of standard node*2 + number of split node*1*2 + number of tip node*4*2. We use fictitious nodes/control points to handle these additional degrees of freedom. At a $H(x)$ enriched node, we add one fantom node and at tip enriched node, four fantom nodes are added. These fictitious nodes are numbered from the total number of true nodes.

In XIGA, the domain consists of split elements, tip elements (enriched elements), and the standard (nonenriched) elements. The enriched elements are the elements that are intersected by the discontinuities such as a crack. The first term in the right-hand side of Eq. (27) evaluates the displacement field using the standard IGA approximation, while the remaining terms are the enrichment approximations to model the discontinuity as well as representing the accurate solution of the displacement field, near the crack tip. On substituting the trial functions, the following discrete system of equations are obtained as,

$$[K]\{d\} = \{F\} \tag{29}$$

where, $[K]$ is the global stiffness matrix, $\{d\}$ is the vector of nodal unknowns and $\{f\}$ is the external force vector. The displacement control variables and the additional enrichment degrees of freedom are as,

$$\boldsymbol{U} = \{u \;\; a \;\; b_1 \;\; b_2 \;\; b_3 \;\; b_4\}^T \tag{30}$$

The global stiffness matrix $\boldsymbol{K}$ is explained as,

$$\boldsymbol{K} = \begin{bmatrix} K_{ij}^{uu} & K_{ij}^{ua} & K_{ij}^{ub} \\ K_{ij}^{au} & K_{ij}^{aa} & K_{ij}^{ab} \\ K_{ij}^{bu} & K_{ij}^{ba} & K_{ij}^{bb} \end{bmatrix} \quad , \quad \mathrm{i,\ j} = 1, 2, 3, \ldots, n_{el} \tag{31}$$

The discretized form of the governing equation is

$$\boldsymbol{K} = \int_\Omega \left(\boldsymbol{B}_i^r\right)^T \boldsymbol{D}\boldsymbol{B}_j^s \, d\Omega \qquad where \quad r,s = u,a,b \tag{32}$$

The global force vector $\boldsymbol{F}$ is expressed as,

$$F_i = \left\{F_i^u \;\; F_i^a \;\; F_i^{b_1} \;\; F_i^{b_2} \;\; F_i^{b_3} \;\; F_i^{b_4}\right\}^T \tag{33}$$

$$\begin{aligned} F_i^u &= \int_{\Omega_e} \boldsymbol{R}_i^T \boldsymbol{b} \, d\Omega + \int_{\Gamma_t} R_i^T \hat{\boldsymbol{t}} \, d\Gamma \\ F_i^a &= \int_{\Omega_e} R_i^T H \boldsymbol{b} \, d\Omega + \int_{\Gamma_t} R_i^T H \hat{\boldsymbol{t}} \, d\Gamma \\ F_i^{b_\alpha} &= \int_{\Omega_e} R_i^T Q_\alpha \boldsymbol{b} \, d\Omega + \int_{\Gamma_t} R_i^T Q_\alpha \hat{\boldsymbol{t}} \, d\Gamma \end{aligned} \tag{34}$$

where in Eq. (32)

$$\boldsymbol{B}_i^u = \begin{bmatrix} R_{i,x_1} & 0 \\ 0 & R_{i,x_2} \\ R_{i,x_2} & R_{i,x_1} \end{bmatrix} \tag{35}$$

$$\boldsymbol{B}_i^a = \begin{bmatrix} (R_i)_{,x_1} H & 0 \\ 0 & (R_i)_{,x_2} H \\ (R_i)_{,x_2} H & (R_i)_{,x_1} H \end{bmatrix} \tag{36}$$

$$\boldsymbol{B}_i^b = \left[B_i^{b_1} \quad B_i^{b_2} \quad B_i^{b_3} \quad B_i^{b_4} \right] \tag{37}$$

$$\boldsymbol{B}_i^{b_\alpha} = \begin{bmatrix} \left(R_i Q_\alpha\right)_{,x_1} & 0 \\ 0 & \left(R_i Q_\alpha\right)_{,x_2} \\ \left(R_i Q_\alpha\right)_{,x_2} & \left(R_i Q_\alpha\right)_{,x_1} \end{bmatrix} \tag{38}$$

and $\alpha = 1, 2, 3, 4$. Finally, by calculating the displacement values, strain and stress values can be obtained using Eq. (52) and (53).

$$[\varepsilon] = [\mathrm{B}]\{\mathrm{d}\} \tag{39}$$

$$[\sigma] = [D][\varepsilon] \tag{40}$$

where $\{d\}$ is the displacement vector, $[D]$ is the Mechanical properties matrix, $[\varepsilon]$ is the strain matrix and $[\sigma]$ is the stress matrix.

3 INTERACTION INTEGRAL AND STRESS INTENSITY FACTOR EVALUATION

In this section, the interaction integral will be derived for extracting SIF (SIFs) along the crack tip. Throughout this work, the material is limited to linear elastic and isotropic conditions, and small strain kinematics is assumed. The interaction integral or *M*-integral is derived from the path independent *J*-integral [24]. The formulation of the *M*-integral is presented here followed by techniques to calculate SIFs.

The path independent *J*-integral [24], is defined as,

$$\mathrm{J} = \lim_{\Gamma \to 0} \int_\Gamma \left(w \delta_{1j} - \sigma_{ij} u_{i,1} \right) n_j d\Gamma \tag{41}$$

where w is the strain energy density defined as:

$$w = \int_0^{\varepsilon_{kl}} \sigma_{ij} \, d\varepsilon_{ij} \tag{42}$$

and n_j denotes the outward normal vector to the contour Γ, as shown in Fig. 4.

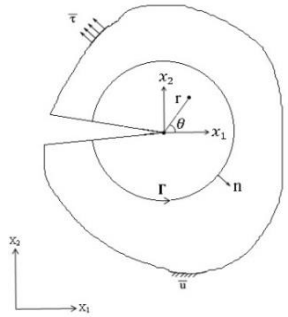

Fig.4
Integration path and coordinate systems. The cartesian (x_1, x_2) and polar (r,θ) coordinate systems located at the crack tip. Notation $\bar{u}$ denotes displacements and $\bar{\tau}$ denotes tractions.

If two supportable and independent fields are considered in a condition that the displacements, strains, and stresses of the actual fields and the auxiliary fields are denoted by (u,ε,σ) and (u^{aux}, ε^{aux},σ^{aux}) respectively, then the *J*-integral of these fields can be defined as:

$$\mathrm{J}^{s}=\int_{\Gamma}\left\{\frac{1}{2}\left(\sigma_{ik}+\sigma_{ik}^{aux}\right)\left(\varepsilon_{ik}+\varepsilon_{ik}^{aux}\right)\delta_{1j}-\left(\sigma_{ij}+\sigma_{ij}^{aux}\right)\left(u_{i,1}+u_{i,1}^{aux}\right)\right\}n_{j}d\Gamma \tag{43}$$

This integral can be decomposed into

$$\mathrm{J}^{s}=\mathrm{J}+\mathrm{J}^{aux}+M \tag{44}$$

where J is given by Eq. (41) and J^{aux} is given by

$$\mathrm{J}^{aux}=\int_{\Gamma}\left(w^{aux}\delta_{1j}-\sigma_{ij}^{aux}u_{i,1}^{aux}\right)n_{j}d\Gamma \tag{45}$$

with

$$w^{aux}=\int_{0}^{\varepsilon_{kl}^{aux}}\sigma_{ij}^{aux}\,d\,\varepsilon_{ij}^{aux} \tag{46}$$

M is the interaction integral including the cross-terms of actual and auxiliary fields, that is defined as:

$$\mathrm{M}=\int_{\Gamma}\left\{\frac{1}{2}\left(\sigma_{ik}\,\varepsilon_{ik}^{aux}+\sigma_{ik}^{aux}\,\varepsilon_{ik}\right)\delta_{1j}-\left(\sigma_{ij}\,u_{i,1}^{aux}+\sigma_{ij}^{aux}u_{i,1}\right)\right\}n_{j}d\Gamma \tag{47}$$

The auxiliary stress fields in polar coordinates are explained as [25]:

$$\sigma_{ij}^{aux}=\frac{K_{I}^{aux}}{\sqrt{2\pi r}}f_{ij}^{I}(\theta)+\frac{K_{II}^{aux}}{\sqrt{2\pi r}}f_{ij}^{II}(\theta)\qquad(i,j=1,2) \tag{48}$$

where the functions $f_{ij}(\theta)$ are provided in [25] and the auxiliary displacement fields are defined as:

$$u_{i}^{aux}=\frac{K_{I}^{aux}}{\mu}\sqrt{\frac{r}{2\pi}}g_{i}^{I}(\theta)+\frac{K_{II}^{aux}}{\mu}\sqrt{\frac{r}{2\pi}}g_{i}^{II}(\theta)\quad(i,j=1,2) \tag{49}$$

where K_{I}^{aux} and K_{II}^{aux} are the auxiliary mode I and mode II SIFs, respectively. The functions $g_i(\theta)$ are also provided in [25]. Moreover, the auxiliary strain fields are explained as:

$$\varepsilon_{ij}=\frac{1}{2}(u_{i,j}^{aux}+u_{j,i}^{aux}) \tag{50}$$

The relationship between J-integral and K_I and K_{II} is defined as [25]:

$$\mathrm{J}=\frac{K_{I}^{2}+K_{II}^{2}}{E'} \tag{51}$$

where $E^{'}$ is defined in terms of E (Young's modulus) and ϑ (poison's ratio) as:

$$E^{'}=\begin{cases}E & \textit{plan stress}\\ \dfrac{E}{\left(1-\vartheta^{2}\right)} & \textit{plane strain}\end{cases} \tag{52}$$

By superposing the actual and auxiliary fields, and using Eq. (51), Eq. (53) obtains as:

$$\mathbf{J}^{s} = \frac{(K_{I} + K_{I}^{aux})^2 + (K_{II} + K_{II}^{aux})^2}{E'} = \mathbf{J} + \mathbf{J}^{aux} + M \tag{53}$$

and

$$M = \frac{2}{E'}\left(K_{I} K_{I}^{aux} + K_{II} K_{II}^{aux}\right) \tag{54}$$

The integral Eq. (47) is not the appropriate form for further evaluations. Thus, it is necessary to recast this integral into a similar domain form. This task would be done by multiplying the integrand by a sufficiently smooth weighting function $q(x)$. This weighting function takes a value of unity on an open set including the crack tip and losses on an outer prescribed contour C_0. Then for each part of contour Γ as shown in Fig. 5, it is assumed that the crack line is traction free and straight in the domain A which is bounded by the contour C_0. Then the interaction integral may be rewritten as,

$$\mathrm{M} = \int_{C} \left\{ \frac{1}{2}\left(\sigma_{ik}\varepsilon_{ik}^{aux} + \sigma_{ik}^{aux}\varepsilon_{ik}\right)\delta_{1j} - \left(\sigma_{ij} u_{i,1}^{aux} + \sigma_{ij}^{aux} u_{i,1}\right) \right\} q m_j d\Gamma \tag{55}$$

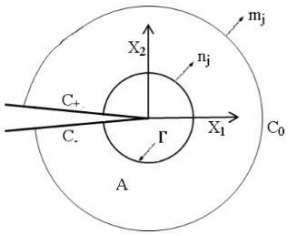

Fig.5
Domain A contains Γ, C_+, C_-, and C_0. Unit normal $m_j = n_j$ on C_+, C_-, and C_0 and $m_j = -n_j$ on Γ.

where contour $C = \Gamma + C_+ + C_- + C_0$ and m is the normal unit outward to the contour C. Now by the divergence theorem and passing to the limit as the contour Γ is miniaturized to the crack tip, gives the Eq. (56) for the interaction integral in domain form,

$$\mathrm{M} = \int_{A} \left\{ \frac{1}{2}\left(\sigma_{ik}\varepsilon_{ik}^{aux} + \sigma_{ik}^{aux}\varepsilon_{ik}\right)\delta_{1j} - \left(\sigma_{ij} u_{i,1}^{aux} + \sigma_{ij}^{aux} u_{i,1}\right) \right\} \frac{dq}{dx_j} dA \tag{56}$$

where $m_j = -n_j$ on Γ and $m_j = n_j$ on C_0, C_+ and C_-.

For the numerical calculation of this integral, domain A is set to be a band of elements around the crack tip. In this study, the first step is determining the characteristic length of an element near the crack tip and designates this quantity as h_{local}. For two dimensional analysis, this value is computed as the square root of the area of the element. Domain A is then allowed to encapsulate all elements with their control points being with a circle of radius r_d around the crack tip. Fig. 6 shows a band of elements for the domain A with the circle domain with radius r_d taken to be twice the length h_{local}. The q function would have a value of unity for all control points within this domain and zero on other control points. The function can be smoothly interpolated within the elements using the nodal shape functions.

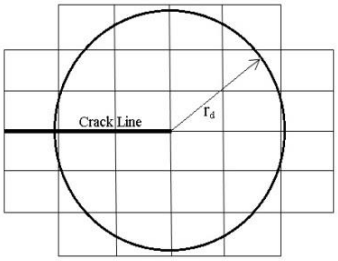

Fig.6
Selected Elements around the crack tip.

4 FATIGUE CRACK GROWTH ANALYSIS

In structures, it is important to be able to predict the rate of the crack growth and the structure's fatigue life during cyclic loading such that a component in operation either can be replaced or repaired before the crack reaches its critical length. In this study, the rate of crack growth is calculated for each crack increment using Paris law which is defined as,

$$\frac{da}{dN} = c\left(\Delta K\right)^m \tag{57}$$

where c and m are Paris low constant parameters and the change in SIF (ΔK) for constant amplitude cyclic load is defined as,

$$\Delta K = K_{max} - K_{min} \tag{58}$$

where K_{max} and K_{min} are the SIFs that correspond to the maximum and minimum value of the applied loads, respectively. After computing the crack growth rate, the numerical integration approach has been employed for calculating the fatigue life which is corresponded to the applied load.

5 THERMO-ELASTIC EQUATIONS

The strain in problems with thermo mechanical loads includes two parts [26],

$$\varepsilon^T = \varepsilon^m + \varepsilon^{th} \tag{59}$$

where ε^m, ε^{th}, and ε^T are mechanical, thermal and total strains, respectively. The thermal strain can be calculated as,

$$\begin{Bmatrix} \varepsilon_{11}^{th} \\ \varepsilon_{22}^{th} \\ 2\varepsilon_{12}^{th} \end{Bmatrix} = \begin{Bmatrix} \alpha_{11} \\ \alpha_{22} \\ 0 \end{Bmatrix} \Delta T \tag{60}$$

where α_{ij} and ΔT are thermal expansion coefficient and temperature gradient, respectively. Furthermore, the mechanical strain is calculated as,

$$\begin{bmatrix} \varepsilon_{11}^{m} \\ \varepsilon_{22}^{m} \\ 2\varepsilon_{12}^{m} \end{bmatrix} = \begin{bmatrix} a_{11} & a_{12} & a_{13} \\ a_{21} & a_{22} & a_{23} \\ a_{31} & a_{32} & a_{33} \end{bmatrix} \begin{bmatrix} \sigma_{11} \\ \sigma_{22} \\ \sigma_{12} \end{bmatrix} \tag{61}$$

The thermal equation can be written as,

$$\boldsymbol{P}\boldsymbol{T}^{h} + \boldsymbol{f}^{th} = 0 \tag{62}$$

where $\boldsymbol{P}$ is the thermal stiffness matrix, $\boldsymbol{f}^{th}$ is the thermal force vector. Also, the temperature vector $\boldsymbol{T}^h$ is defined as,

$$\boldsymbol{T}^{h} = \begin{Bmatrix} u & a & b_1 \end{Bmatrix} \tag{63}$$

The thermal stiffness matrix $\boldsymbol{P}$ and the thermal force vector $\boldsymbol{f}^{th}$ Calculated as:

$$\boldsymbol{f}^{th} = \left\{ f^{th-u} \quad f^{th-a} \quad f^{th-b_1} \right\} \tag{64}$$

$$\boldsymbol{P}^{rs} = \int_{\Omega} \left(\boldsymbol{B}^{th-r} \right)^{T} \boldsymbol{D}^{th} \boldsymbol{B}^{th-s} d\Omega + \int h \boldsymbol{R}^{T} \boldsymbol{R} \, dS \qquad ,(r,s = u,a,b) \tag{65}$$

$$F_i^{th-u} = \int \boldsymbol{R}_i^T \boldsymbol{Q} \, d\Omega + \int \boldsymbol{R}_i^T \boldsymbol{q} \, dS + \int \boldsymbol{R}_i^T h T_\infty \, dS \tag{66}$$

$$F_i^{th-a} = \int \boldsymbol{R}_i^T H \boldsymbol{Q} \, d\Omega + \int \boldsymbol{R}_i^T H \boldsymbol{q} \, dS + \int \boldsymbol{R}_i^T H h T_\infty \, dS \tag{67}$$

$$F_i^{th-b_1} = \int \boldsymbol{R}_i^T Q_{th} \boldsymbol{Q} \, d\Omega + \int \boldsymbol{R}_i^T Q_{th} \boldsymbol{q} \, dS + \int \boldsymbol{R}_i^T Q_{th} h T_\infty \, dS \tag{68}$$

The matrices of basis functions derivatives are defined as:

$$\boldsymbol{B}_i^{th-u} = \begin{bmatrix} R_{i,x_1} \\ R_{i,x_2} \end{bmatrix} \tag{69}$$

$$\boldsymbol{B}_i^{th-a} = \begin{bmatrix} (R_i)_{,x_1} H \\ (R_i)_{,x_2} H \end{bmatrix} \tag{70}$$

$$\boldsymbol{B}_i^{th-b_1} = \begin{bmatrix} (R_i Q_{th})_{,x_1} \\ (R_i Q_{th})_{,x_2} \end{bmatrix} \tag{71}$$

where Q_{th} is asymptotic thermal crack tip enrichment function as:

$$Q_{th} = \left\{ \sqrt{r} \sin \frac{\theta}{2} \right\} \tag{72}$$

By solving the thermal Eq. (71), the thermal strain can be computed by Eq. (69) using temperature values. Moreover, the total force vector in Eq. (29) can be defined as:

$$f = f^{th} + f^{m} = \int_{\Omega} B^T D \varepsilon^{th} d\Omega + f^{m} \tag{73}$$

where the B matrix is presented as Eq. (35) to Eq. (38).

Finally, using both indicated total force and Eq. (29) could lead to the calculation of the total strain.

6 NUMERICAL EXAMPLES

To demonstrate the accuracy and verify the convergence of the proposed method, some numerical example of fracture problems for the isotropic materials has been solved. Presented numerical example were two isotropic problems as, (I) an edge cracked plate (Fig. 7(a)), and (II) a center cracked plate that both of them subjected to uniform tension, (Fig. 7(b)).

Stress intensity factor results are independent of material constants. The constants of used material are as Young's modulus E = 207 *GPa* and Poisson's ratio = 0.3. The evaluated models are of unit thickness. The material is assumed to be the plane strain and analysis in linear elastic fracture mechanic. For the sake of convenience, the M-integral values are converted to stress intensity factor. In this study, exact solutions of the stress intensity factor are also calculated.

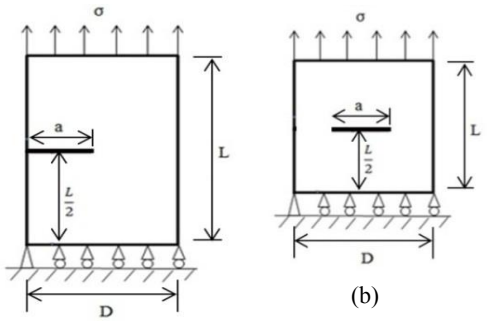

Fig.7
The edge cracked plate and the center cracked plate.

6.1 Edge cracked plate

Consider the geometry shown in Fig. 7(a), a plate of width D and height L with an edge crack of length a, that values are given in Table 1. Moreover, mechanical and thermal load and boundary condition are specified in Table 1 and Fig. 7(a).

In this study, the properties of material are temperature independent. The values of Physical, mechanical and thermal properties of material are in room temperature.

Table 1
Dimensions and condition of the edge cracked plate.

Specifications	Measure
Plate length	400 *mm*
Plate width	200 *mm*
Crack length	95 *mm*
Applied stress	1000 *KPa*
Top edge(Heat flux)	1000 W/m^2
Bottom edge(Constant temperature)	60^oc
Left edge	Insulated
Right edge	Insulated
Heat conductivity	50 W/m^oK
Thermal expansion coefficient	15e-6 $1/^oC$

Using basis functions and proper control points, the geometry of the plate is formed and then the crack is created at the desired position. To show the effect of refinement operation on the convergence rate and results, present problem is solved for linear (p=q=1), quadratic (p=q=2) and cubic (p=q=3) basis functions. In addition, by definition the appropriate level set function, the control points around the crack line and the crack tip are identified. After calculating the total stiffness matrix, enrichment of control points around the crack line and the crack tip, applying boundary conditions and force, displacement and consequently strain and stress values for each element and related control points are obtained. To validate the results of XIGA method, finite element solving of the problem has been done. Contour plot from the extended IGA based on Bézier extraction method and the finite element method are shown in Fig. 8. The results obtained from the solution with XIGA based on Bézier extraction and finite element methods are presented in Table 2. Based on the results, the convergence study and comparison between the XIGA based on Bézier extraction and finite element methods are shown in Fig. 9.

Table 2
Maximum displacement in X and Y direction (m)$\times 10^{-5}$ and Maximum von Mises stress $\sigma_{von}\times 10^7$ (pa).

FEM				Bézier XIGA, (p=q=1)			
No. of elements	U_x^{max}	U_y^{max}	σ_{von}^{max}	No. of elements	U_x^{max}	U_y^{max}	σ_{von}^{max}
129	7.2913	7.2957	2.8026	48	7.3356	7.3921	5.9963
191	7.7848	7.6982	4.3082	140	7.7918	7.7267	7.7428
324	8.0084	7.8799	6.4046	600	8.0860	7.9471	9.9254
639	8.1597	8.0010	8.1495	1800	8.1978	8.0317	12.185
2356	8.2159	8.0467	12.628	4200	8.2349	8.0637	16.795
42474	8.2551	8.0784	18.144	16200	8.2574	8.0803	25.293
166216	8.2582	8.0806	26.736	25200	8.2608	8.0820	26.642

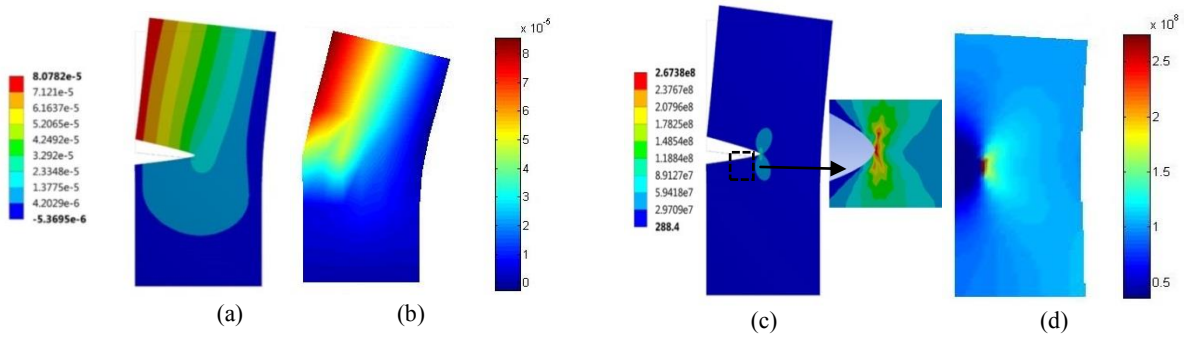

Fig.8
Comparing the results of isogeometric analysis and finite element analysis. (a) Finite element displacement in *Y* direction (*mm*). (b) Isogeometric displacement in *Y* direction (*mm*). (c) Finite element von Mises stress (*Pa*). (d) Isogeometric von Mises stress (*Pa*).

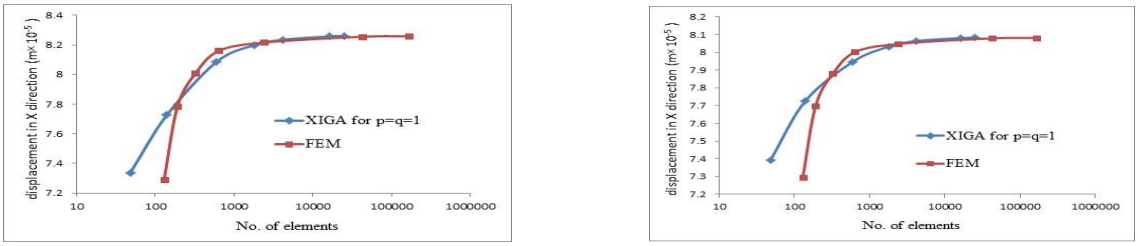

Fig.9
Convergence study and comparison of maximum displacement in (a) *X* direction and (b) *Y* direction.

After obtaining the above results, the stress intensity factor at the crack tip is calculated using the interaction integral. The exact solution (analytical) for calculating the stress intensity factor of the first mode for a plate with edge crack is obtained using the following equation [27]:

$$K_I = \left[1.12 - 0.23\left(\frac{a}{D}\right) + 10.55\left(\frac{a}{D}\right)^2 - 21.72\left(\frac{a}{D}\right)^3 + 30.39\left(\frac{a}{D}\right)^4\right]\sigma\sqrt{\pi a} \tag{74}$$

where a, is the length of the crack and D is the width of the plate. The results obtained for the SIF from the XIGA based on Bézier extraction, FEM and the exact solution are presented in Table 3. In this table the exact solution is equal to 1.4261. The accuracy of all results is excellent, there is less than 1 percent variation among all configurations tested in the convergence range.

Table 3
Stress intensity factor (K_I), $(pa\sqrt{\boldsymbol{m}})\times 10^7$.

FEM			Bézier XIGA, (p=q=1)			Bézier XIGA, (p=q=2)			Bézier XIGA, (p=q=3)		
No. of elements	K	Error	No. of elements	K	Error	No. of elements	K	Error	No. of elements	K	Error
129	1.0333	%27.54	48	1.2617	%11.52	45	1.2498	%12.36	44	1.2385	%13.15
191	1.3003	%8.82	140	1.3707	%3.88	70	1.3186	%7.54	52	1.3021	%10.09
344	1.3604	%4.61	600	1.4081	%1.54	150	1.3651	%4.28	64	1.3523	% 5.17
639	1.3832	%3.01	1800	1.4160	%0.63	375	1.4034	%1.59	76	1.3948	%3.94
2356	1.4059	%1.42	4200	1.4194	%0.46	750	1.4179	%0.87	90	1.4195	%0.46
42474	1.4196	%0.46	16200	1.4239	%0.15	1125	1.4249	%0.08	128	1.4235	%0.02
166216	1.4235	%0.15	25200	1.4254	%0.04	1500	1.4264	%0.01	156	1.4263	%0.01

The study of convergence and comparison of the values for stress intensity factor based on XIGA (with the knot insertion and increase in the number of elements) and the FEM is shown in Fig. 10(a). The values of stress intensity factor from solving with the XIGA with order elevation (p-refinement) for p=q=1, p=q=2, and p=q=3, and the exact

solution are presented in Fig. 10(b). The results show that the application of p-refinement produces higher precision results with lower computational costs.

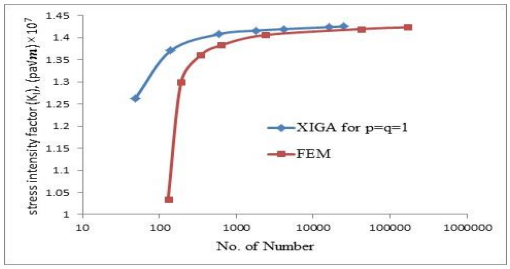

(a)

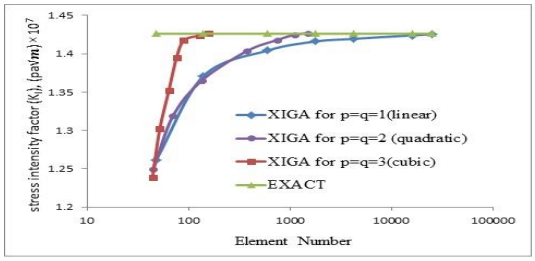

(b)

Fig.10
(a) Convergence study and comparison of stress intensity factor (K_I). (b) Comparison of stress intensity factor (K_I) for p=q=1, p=q=2 and p=q=3.

The calculation of the SIF in the present problem is solved for different crack lengths by XIGA method and finite element methods, and the results are compared with the exact solution. Results and comparisons are presented in Table 4 and Fig. 11(a).

Table 4
Stress intensity factor (K_I), ($pa\sqrt{\boldsymbol{m}}$)× 10^7 for different crack lengths.

crack length (m)	Exact	Bézier XIGA	Error	FEM	Error
0.095	1.4261	1.4239	% 0.15	1.4235	% 0.18
0.105	1.7649	1.7565	% 0.47	1.7252	% 2.25
0.115	2.2051	2.1941	% 0.49	2.1413	% 2.89
0.125	2.7772	2.7768	% 0.01	2.6896	% 3.15
0.135	3.5170	3.6017	% 2.71	3.3974	% 3.41

Now, the fatigue life of an edge cracked plate is evaluated by extended IGA method. The thermal load, thermal and mechanical boundary conditions, control net and crack increment are kept the same as above. The mechanical load has a zero base as σ_{min}= 0 and σ_{max}=1000 *Kpa* at the top edge of the plate. This problem is also solved by the finite element method using quadrilateral elements for a uniform mesh.

The fatigue life of an edge cracked plate is evaluated by Paris law. The Paris constant of material considered as $C = 2.087\times10^{-12}\,\frac{mm}{cycle}\left(\mathrm{MPa}\sqrt{\mathrm{m}}\right)^{-\mathrm{m}}$ and m=3. Also, the critical SIF (K_{IC}) is equal to $80\,MPa\sqrt{m}$. In this study, initial crack length considered to be 20 *mm* and the crack length increment coefficient for each iteration is c=1.1($a_n = a_{n-1} + \left(0.1\times a_0\right)$) until reaching the critical stress intensity factor. A comparison of fatigue life obtained by extended IGA and finite element methods is shown in Fig. 11(b). The fatigue life of the plate obtained by XIGA is found to be 399,374 cycles, whereas the fatigue life obtained by finite element is found to be 385,457 cycles. The crack growth paths obtained by both two methods are nearly a straight path.

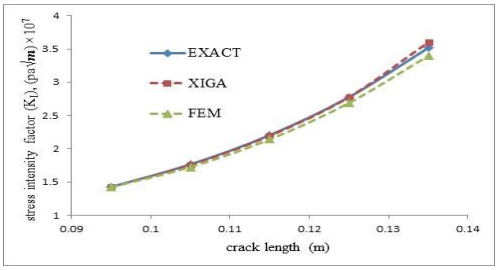

(a)

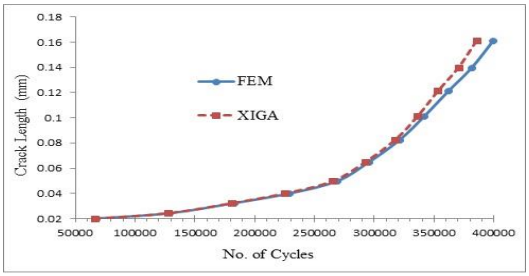

(b)

Fig.11
(a)Comparison of stress intensity factor (K_I) for different crack lengths. (b) Fatigue life variation with the crack length for an edge cracked plate.

6.2 Center cracked plate

For the next example, consider the center cracked plate shown in Fig. 7(b), a plate with width D, height L and a center crack of length a, that values are given in Table 5 mechanical and thermal load and boundary condition are specified in Table 5 and Fig. 7(b).

Table 5
Dimensions and condition of the edge cracked plate.

Specifications	Measure
Plate length	200 *mm*
Plate width	200 *mm*
Crack length	95 *mm*
Applied stress	1000 *KPa*
Top edge(Heat flux)	1000 W/m^2
Bottom edge(Constant temperature)	60^oc
Left edge	Insulated
Right edge	Insulated
Heat conductivity	50 W/m^oK
Thermal expansion coefficient	15e-6 $1/^oC$

All analyzes that done for the edge cracked plate, for the center cracked plate were performed as well, and the results are shown in Figs. 12- 15 and Tables 6-8.

Table 6
Maximum displacement in X and Y direction $(m)\times 10^{-5}$ and Maximum stress in Y direction $\sigma_y \times 10^7$ (pa).

FEM				Bézier XIGA, $(p=q=1)$			
No. of elements	U_x^{max}	U_y^{max}	σ_{von}^{max}	No. of elements	U_x^{max}	U_y^{max}	σ_y^{max}
64	5.8325	5.5156	0.0626	36	6.0183	5.0183	0.0899
96	6.4529	6.1997	0.1082	100	6.5817	6.5817	0.1128
163	6.7245	6.8673	1.1989	625	7.0292	7.0292	1.0254
325	6.9116	7.1184	1.9985	1600	7.1329	7.1529	2.0081
1132	7.1223	7.2016	2.9367	3025	7.1693	7.1993	2.9859
21319	7.1829	7.2529	3.5941	7225	7.1942	7.2262	3.2819
84211	7.1992	7.2644	3.7016	13225	7.2008	7.2308	3.6420

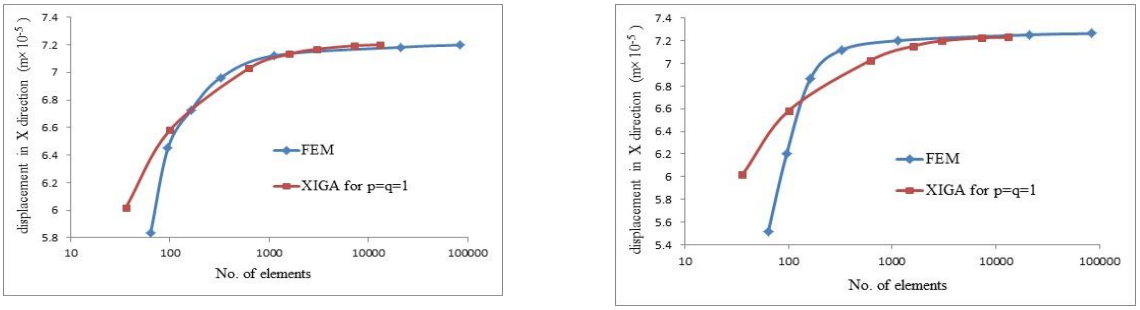

(a) (b)

Fig.12
Convergence study and comparison of maximum displacement in (a) X direction and (b) Y direction.

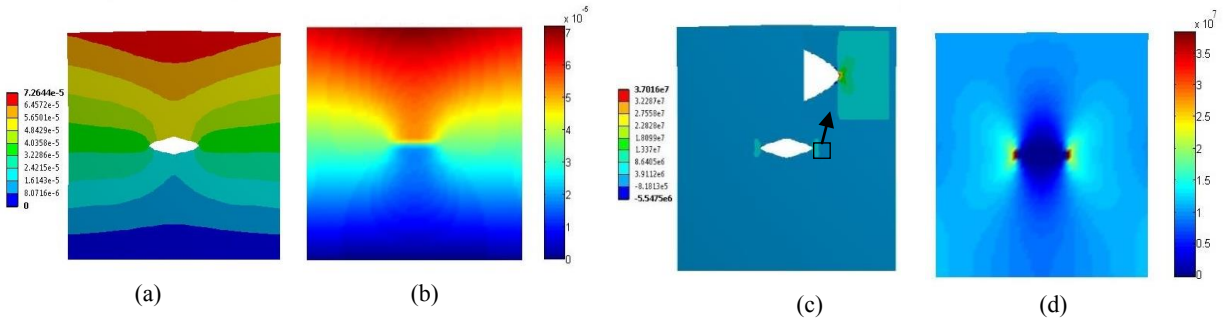

(a) (b) (c) (d)

Fig.13
Comparing the results of isogeometric analysis and finite element analysis. (a) Finite element displacement in *Y* direction (*mm*). (b) Isogeometric displacement in *Y* direction (*mm*). (c) Finite element stress in *Y* direction (*Pa*). (d) Isogeometric stress in *Y* direction (*Pa*).

Convergence study of stress intensity factor for XIGA based on Bézier extraction and FEM is shown in Fig. 14(a). Comparison of stress intensity factor values from extended IGA method with order elevation (*P*-refinement) for $p=q=1$, $p=q=2$, and $p=q=3$, and the exact solution are presented in Fig. 14(b). This figure shows that *p*-refinement cause Results obtained with high precision and lower computational cost. The exact solution for the first mode SIF is obtained using the following equation [27]:

$$K_I = \left[\left(1-\left(\frac{a}{2D}\right)+0.326\left(\frac{a}{D}\right)^2\right)\div\sqrt{1-\left(\frac{a}{D}\right)}\right]\sigma\sqrt{\pi a} \tag{75}$$

where a, is the length of the crack and D is the width of the plate. The exact solution for the stress intensity factor is equal to 0.9998.

Table 7
Stress intensity factor (K_I), $(pa\sqrt{\boldsymbol{m}})\times 10^7$.

FEM			Bézier XIGA, ($p=q=1$)			Bézier XIGA, ($p=q=2$)			Bézier XIGA, ($p=q=3$)		
No. of elements	*K*	Error	No. of elements	*K*	Error	No. of elements	*K*	Error	No. of elements	*K*	Error
64	0.5038	%49.61	36	0.6187	%38.12	36	0.6894	%31.05	25	0.7158	%28.41
96	0.6403	%35.96	100	0.7529	%24.69	64	0.7925	%20.73	36	0.8074	%19.24
163	0.8344	%16.54	625	0.9095	%9.03	100	0.8812	%11.88	49	0.8949	%10.04
325	0.9022	%9.76	1600	0.9564	%4.34	225	0.9598	%4.00	64	0.9418	%5.80
1132	0.9589	%4.10	3025	0.9783	%2.15	625	0.9916	%0.82	81	0.9958	%0.40
21319	0.9796	%3.02	7225	0.9889	%1.02	900	0.9976	%0.21	100	0.9997	%0.01
84211	0.9868	%1.03	13225	0.9931	%0.67	1089	0.9989	%0.08	121	1.0002	%0.03

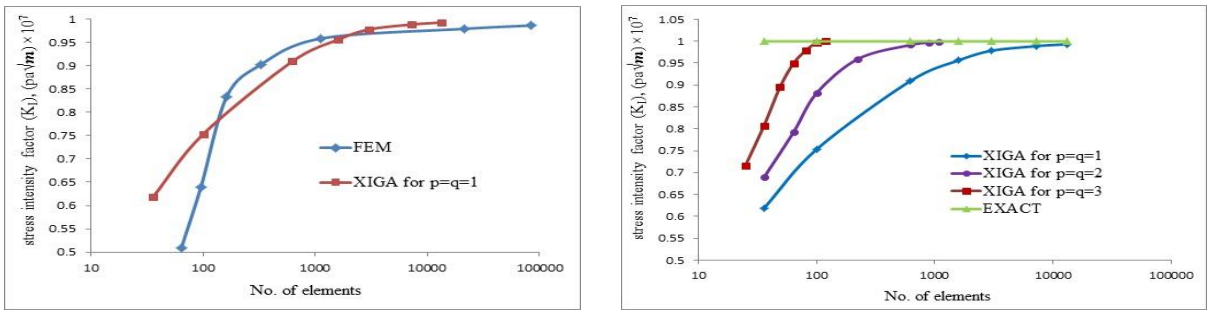

(a) (b)

Fig.14
(a) Convergence study and comparison of stress intensity factor (K_I). (b) Comparison of stress intensity factor (K_I) for $p=q=1$, $p=q=2$ and $p=q=3$.

The result of stress intensity factor for different crack lengths by extended IGA, finite element, and the exact solution are presented in Table 8 and compared in Fig. 15(a).

Table 8
Stress intensity factor (K_I), ($pa\sqrt{\boldsymbol{m}}$)$\times 10^7$ for different crack lengths.

crack length (m)	Exact	Bézier XIGA	Error	FEM	Error
0.095	0.9998	0.9869	% 1.02	0.9791	% 1.03
0.105	1.3165	1.3204	% 0.47	1.3011	% 2.25
0.115	1.8239	1.8321	% 0.49	1.7984	% 2.89
0.125	2.3196	2.3414	% 0.01	2.2796	% 3.15
0.135	2.9859	3.0311	% 2.71	2.9212	% 3.41

The fatigue life of a center cracked plate is evaluated by extended IGA method and finite element method. The thermal and mechanical load, thermal and mechanical boundary conditions, crack increment and all other conditions are kept the same as edge cracked plate. A comparison of fatigue life obtained by extended IGA and finite element methods is shown in Fig. 15(b).

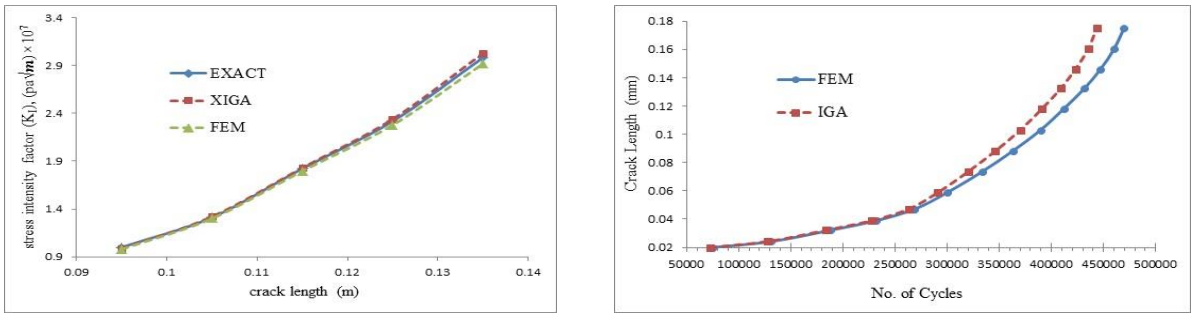

(a) (b)

Fig.15
(a)Comparison of stress intensity factor (K_I) for different crack lengths. (b) Fatigue life variation with the crack length for a center cracked plate.

7 CONCLUSIONS

In the present work, extended isogeometric method based on Bézier extraction has been used for analyzes of plane crack problems under thermal and mechanical cyclic loading. We investigated the advantages and rectified the drawbacks of the approach, and proposed some improvements to the procedure, which makes the approach amenable to realistic damage tolerance assessment problems. We have used the interaction integral, to estimate SIF and Paris law, to evaluate the fatigue life in linear elastic fracture mechanics. Furthermore, the level set method has been developed to identify grid points around the crack line and crack tip then added discontinuous enrichment functions to the IGA approximation and modeling crack growth without remeshing. Some numerical example has been solved to check the accuracy of the presented approach to predict the SIF and fatigue life. Based on the present work, the following conclusions are drawn,

- In all examples, good agreements between the two solutions are found. The extended isogeometric method based on Bézier extraction has been found quite effective, useful and more accurate and beneficial to compute the stress intensity factor and the fatigue life of crack problems. Moreover, the saving in CPU is quite significant in this method.
- The proposed integration scheme preserves the accuracy for highly distorted elements or control points which commonly arise in isogeometric analysis.
- The fatigue life of an edge crack plate is found small as compared to the center crack plate under the same loading and boundary conditions.
- These analyses show that the accuracy achieved using this method with higher-order basis function found more as compared to the finite element method. The IGA based on Bézier extraction with higher-order

approximations required fewer degrees of freedom than lower-order finite elements for solutions with the same accuracy.

- Because of the Bézier decomposition process (creating piecewise C^0 Bézier elements), k-refinement is not applicable in the isogeometric analysis based on Bézier extraction. Actually, in this method, k-refinement is equivalent to order elevation (*p*-refinement).
- The present IGA based on Bézier extraction of NURBS or another type of basis function could be enhanced by enrichments in the framework of the partition of unity to solve discontinuous problems.

ACKNOWLEDGMENTS

The authors reserve their utmost gratitude for Advanced Computing Center of Ahwaz Islamic Azad University for their collaborate and encourage.

REFERENCES

[1] Sancho J.M., Planas J., Cendón D.A., Reyes E., Gálvez J., 2007, An embedded crack model for finite element analysis of concrete fracture, *Engineering Fracture Mechanics* **74**(1-2): 75-86.

[2] Rabczuk T., Gracie R., Song J.H., Belytschko T., 2010, Immersed particle method for fluid–structure interaction, *International Journal for Numerical Methods in Engineering* **81**(1): 48-71.

[3] Chessa J., Belytschko T., 2003, An enriched finite element method and level sets for axisymmetric two-phase flow with surface tension, *International Journal for Numerical Methods in Engineering* **58**(13): 2041-2064.

[4] Duddu R., Bordas S., Chopp D., Moran B., 2008, A combined extended finite element and level set method for biofilm growth, *International Journal for Numerical Methods in Engineering* **74**(5): 848-870.

[5] Bordas S., Moran B., 2006, Enriched finite elements and level sets for damage tolerance assessment of complex structures, *Engineering Fracture Mechanics* **73**(9): 1176-1201.

[6] Rabczuk T., Belytschko T., 2005, Adaptivity for structured meshfree particle methods in 2D and 3D, *International Journal for Numerical Methods in Engineering* **63**(11): 1559-1582.

[7] Rabczuk T., Zi G., 2007, A meshfree method based on the local partition of unity for cohesive cracks, *Computational Mechanics* **39**(6): 743-760.

[8] Rabczuk T., Xiao S.P., Sauer M., 2006, Coupling of mesh-free methods with finite elements: basic concepts and test results, *Communications in Numerical Methods in Engineering* **22**(10): 1031-1065.

[9] Nguyen-Thanh N., Nguyen-Xuan H., Bordas S.P.A., Rabczuk T., 2011, Isogeometric analysis using polynomial splines over hierarchical T-meshes for two-dimensional elastic solids, *Computer Methods in Applied Mechanics and Engineering* **200**(21-22): 1892-1908.

[10] Bhardwaj G., Singh S., Singh I., Mishra B., Rabczuk T., 2016, Fatigue crack growth analysis of an interfacial crack in heterogeneous materials using homogenized XIGA, *Theoretical and Applied Fracture Mechanics* **85**: 294-319.

[11] Bhardwaj G., Singh I., Mishra B., Bui T., 2015, Numerical simulation of functionally graded cracked plates using NURBS based XIGA under different loads and boundary conditions, *Composite Structures* **126**: 347-359.

[12] Tran L.V., Ferreira A., Nguyen-Xuan H., 2013, Isogeometric analysis of functionally graded plates using higher-order shear deformation theory, *Composites Part B: Engineering* **51**: 368-383.

[13] Huang X., Liu Y., Huang X., 2019, Analytical characterizations of crack tip plastic zone size for central-cracked unstiffened and stiffened plates under biaxial loading, *Engineering Fracture Mechanics* **206**: 1-20.

[14] Gadallah R., Osawa N., Tanaka S., Tsutsumi S., 2018, A novel approach to evaluate mixed-mode SIFs for a through-thickness crack in a welding residual stress field using an effective welding simulation method, *Engineering Fracture Mechanics* **197**: 48-65.

[15] Yuan H., Liu W., Xie Y., 2019, Mode-I stress intensity factors for cracked special-shaped shells under bending, *Engineering Fracture Mechanics* **207**: 131-148.

[16] Cimrman R., Novák M., Kolman R., Tůma M., Plešek J., Vackář J., 2018, Convergence study of isogeometric analysis based on Bézier extraction in electronic structure calculations, *Applied Mathematics and Computation* **319**: 138-152.

[17] Nguyen L.B., Thai C.H., Zenkour A., Nguyen-Xuan H., 2019, An isogeometric Bézier finite element method for vibration analysis of functionally graded piezoelectric material porous plates, *International Journal of Mechanical Sciences* **157**: 165-183.

[18] Singh A.K., Jameel A., Harmain G., 2018, Investigations on crack tip plastic zones by the extended iso-geometric analysis, *Materials Today: Proceedings* **5**(9): 19284-19293.

[19] Yin S., Yu T., Bui T.Q., Zheng X., Gu S., 2019, Static and dynamic fracture analysis in elastic solids using a multiscale extended isogeometric analysis, *Engineering Fracture Mechanics* **207**: 109-130.

[20] Piegl L., Tiller W., 2012, *The NURBS Book*, Springer Science & Business Media, Berlin/Heidelberg, Germany.
[21] Shi J., Chopp D., Lua J., Sukumar N., Belytschko T., 2010, Abaqus implementation of extended finite element method using a level set representation for three-dimensional fatigue crack growth and life predictions, *Engineering Fracture Mechanics* **77**(14): 2840-2863.
[22] Sutradhar A., Paulino G.H., 2004, Symmetric Galerkin boundary element computation of T-stress and stress intensity factors for mixed-mode cracks by the interaction integral method, *Engineering Analysis with Boundary Elements* **28**(11): 1335-1350.
[23] Bremberg D., Faleskog J., 2015, A numerical procedure for interaction integrals developed for curved cracks of general shape in 3-D, *International Journal of Solids and Structures* **62**: 144-157.
[24] de Klerk A., Visser A., Groenwold A.A., 2008, Lower and upper bound estimation of isotropic and orthotropic fracture mechanics problems using elements with rotational degrees of freedom, *Communications in Numerical Methods in Engineering* **24**(5): 335-353.
[25] Sutradhar A., Paulino G. H., 2004, Symmetric Galerkin boundary element computation of T-stress and stress intensity factors for mixed-mode cracks by the interaction integral method, *Engineering Analysis with Boundary Elements* **28**(11): 1335-1350.
[26] Bayesteh H., Afshar A., Mohammdi S., 2015, Thermo-mechanical fracture study of inhomogeneous cracked solids by the extended isogeometric analysis method, *European Journal of Mechanics-A/Solids* **51**: 123-139.
[27] Dowling N.E., 1999, *Mechanical Behavior of Materials: Engineering Methods for Deformation, Fracture, and Fatigue*, Pearson, London, United Kingdom.